Proceedings of the ASME 2020 International Design Engineering Technical Conferences & Computers and Information in Engineering Conference
IDETC/CIE 2020
August 16-19, 2020, St. Louis, MO, USA

DETC2020-22342

TEMPERATURE CONTROL TO INCREASE INTER-LAYER BONDING STRENGTH IN FUSED DEPOSITION MODELLING

Raoul Kumrai-Woodruff
Department of Engineering
Durham University
Durham, United Kingdom

Qing Wang
Department of Engineering
Durham University
Durham, United Kingdom

ABSTRACT

Fused Deposition Modelling (FDM) provides opportunities for new development in numerous areas. Z-directional anisotropic strength caused by weak inter-layer bonding has been recognized as the reason for limited industry adoption of FDM. This paper aims to investigate increasing the Z-directional strength of Acrylonitrile Butadiene Styrene (ABS) using a temperature controlled print environment. The ambient temperature during printing was increased to reduce heat transfer from the print, thereby encouraging more polymer chain inter-diffusion between layers. Dogbone specimens were printed at ambient print temperatures between 24.8°C and 71.2°C and tensile tests were performed. A thermal camera was used to identify heat loss in the FDM process. Ultimate tensile strength was found to increase by a maximum of 104% compared to open enclosure printing. A stylus profiler and scanning electron microscopy were used to compare the quality of the inter-layer bonds, suggesting that additional polymer inter-diffusion occurred at hotter ambient temperatures. A weak positive relationship was found between ambient air temperature and inter-layer part strength. Further experimentation could provide scope to determine an ideal ambient print temperature that is likely to be dependent on print settings and the printer used.

1. INTRODUCTION

Additive Manufacturing (AM), more commonly known as 3D printing, was invented in 1986 [1]. It has five advantages over traditional subtractive manufacturing methods: cost, speed, quality, design potential, and impact [2]. AM has provided new opportunities for development in areas such as aerospace [3], chemistry [4] and medical surgery [5]. Recently, Rolls-Royce redesigned new parts efficiently using 3D printing, to develop the Advance3 demonstrator engine, with the aim of delivering 25% increased fuel efficiency [6]. There are several varieties of AM, such as Stereolithography and Selective Laser Sintering [7], with the most common being Fused Deposition Modelling (FDM) [8]. The print process is similar for all AM methods. A CAD model is sliced into two dimensional layers, which are then consecutively printed. The FDM print process is illustrated in Figure 1.

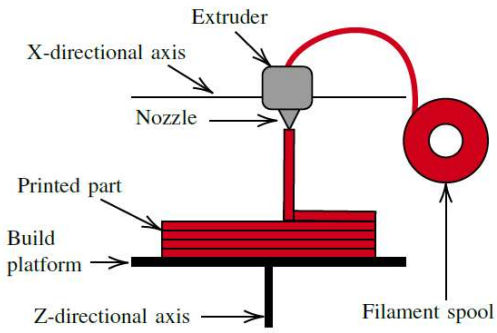

Figure 1: FDM print process illustrated in two dimensions

Filament stored in a spool is pulled through and heated by an extruder head. Next, the heated filament is extruded through a nozzle and deposited in layers on the build platform, via an extruder head moving in the X-Y plane, usually along gantries. The build platform of the printer used to investigate inter-layer strength is lowered after the completion of each layer. The FDM process facilitates the manufacture of previously impossible geometries, leading to part benefits such as stronger and lighter structures [9]. This is due to the ability to prescribe local properties, such as density, upon part fabrication [10]. Furthermore, part lifespan can be improved by using more durable material during manufacture, as well as producing small quantities for bespoke components where required [11]. For FDM to move from a prototyping to a manufacturing method, the mechanical properties, dimensional control and surface finish of parts must be improved [12]. One of the limiting factors in industry adoption of FDM is weak inter-layer bonding [13]. This causes anisotropic strength in the Z-direction. If this

problem could be solved there is potential for FDM to expand into new applications. This paper aims to increase the Z-directional strength of parts produced from an Acrylonitrile Butadiene Styrene (ABS) filament by controlling the ambient air temperature of a MakerBot Replicator 2X printer. Ambient temperature control is hypothesised to decrease heat transfer away from the printed part, resulting in a stronger Z-directional strength. An explanation behind this is provided in Section 2.

2. THEORY

2.1 Polymer Bonding

As described in Section 1, a thermoplastic filament is heated and extruded during the FDM process. This type of material is characterised by two temperatures: the melting temperature and the glass transition temperature. The latter is the transitional temperature between a hard and solid material to a viscous and soft one. It occurs before the melting point. At the start of the FDM print process, the filament begins as hard and solid in the filament spool. When it exits the extruder it has been heated to above its glass transition temperature but below its melting point. This allows the FDM process to deposit filament on the build platform in the desired geometry, whilst still retaining its shape after the extruder head moves away. ABS is a thermoplastic polymer widely used in industry due to its high impact resistance, processability and stability [14]. It is the filament selected for investigation in this paper.

In order to improve Z-directional strength in ABS-printed parts, the cause of anisotropic strength in the FDM process must be understood. Sun et al. (2007) explained that the bonding mechanism is driven by thermal fusion and polymer inter-diffusion of extruded material [12]. The three stages of polymer bonding are illustrated in Figure 2, using two adjacent polymer trails. In Stage 1, shown in Figure 2(a), polymer is extruded adjacent to the previous trail with surface inhomogeneity disappearing, allowing free movement of polymer chains. Stages 2 and 3, shown in Figure 2(b) and Figure 2(c) respectively, are described by the De Gennes reputation model [15]. In Stage 2, neck growth occurs, forming a region where polymer from each trail can diffuse. Diffusion occurs through the random movement of molecules, known as Brownian motion. For a thermoplastic polymer, this occurs above its glass transition temperature. In Stage 3, polymer chain inter-diffusion occurs, forming bonds.

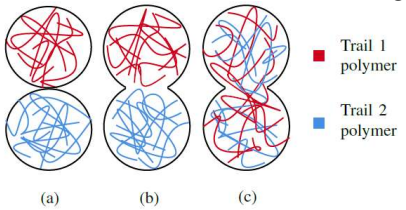

Figure 2: Polymer chain diffusion stages. (a) surface contacting, (b) neck growth, (c) polymer inter-diffusion

Polymer bond strength is dependent on how much polymer inter-diffusion occurs. Z-directional anisotropic strength is due to weak inter-layer bonds because of insufficient layer polymer inter-diffusion. This is due to each print layer quickly cooling down during printing. A print layer can take several seconds, so heat is lost and less thermal energy is available to drive the polymer bonding mechanism between layers, whereas within each layer, polymer trails are deposited next to each other, microseconds apart. More heat is retained so more polymer inter-diffusion occurs, leading to stronger bonds in the X and Y directions. To increase Z-directional strength, more polymer inter-diffusion needs to occur between layers. This mechanism is driven by thermal energy [12]. If the print can retain more heat between layers, more polymer inter-diffusion will occur. Section 2.2 describes the heat transfer in the FDM process.

2.2 Heat Transfer

Conduction, convection and radiation are the three modes of heat transfer. Conduction is heat transfer through physical contact whilst radiation is heat transfer through electromagnetic waves. The dominant fluid heat transfer mode is convection, which is the transfer of heat by fluid motion. The two types of convection are natural and forced. Natural convection occurs when fluid motion is driven by buoyancy forces arising from density disparities. Fluid that has been heated expands due to molecules driving each other apart, reducing its density and causing it to rise. This hot fluid displaces colder fluid downwards, causing heat transfer. A convection current, shown in Figure 3, is formed from cold fluid drawn to where hot fluid has risen. The cold fluid is heated by the same source and the process repeats, forming a convection current. Forced convection is the second type of convection, occurring when an internal source, such as a fan or pump, drives fluid flow.

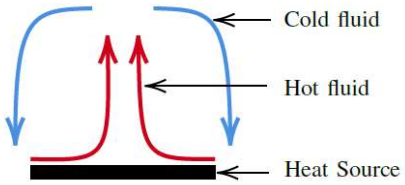

Figure 3: Convection current transferring heat

The MakerBot Replicator 2X printer used in this project is an enclosed printer with side panels and a top cover. Both natural and forced convection occur during the FDM process. This is known as mixed convection. Natural convection occurs during the FDM process when filament is extruded through the print nozzle and deposited on the build plate. The filament temperature at extrusion from the nozzle is around 230°C for ABS printing. This raises the temperature of the surrounding ambient air, forming a convection current. This paper hypothesises that if the heat transfer rate away from the part is decreased, more heat will be retained by the extruded filament. This will increase the amount of polymer inter-diffusion between layers, as explained in Section 2.1, thereby forming stronger inter-layer bonds and leading to increased Z-directional strength. The three main sources of forced convection in the printer are detailed in Table 1.

Table 1: Convection sources within the print enclosure

Source	How convection occurs
Extruder fans	Mounted on extruder blocks to draw heat away, causing air motion at the top of the enclosure
Extruder head	Moved along X-Y gantries during the print process. This pushes air around the enclosure
Heated print bed	Heated to 120 ℃ to reduce warpage of ABS prints. It acts as an additional heat source heating air to form a convection current around the enclosure.

Newton's law of cooling gives a relationship for convective heat transfer from an object, and is provided in Equation 1 [16]. $\dot{Q}$ is the rate of heat transferred (J/s), h is the heat transfer coefficient (W/(m^{2}K)), A is the surface area of the object transferring heat (m^2) and ΔT is the temperature difference between ambient fluid and the surface of the object.

$$\dot{Q} = h\mathrm{A}\Delta\mathrm{T} \quad (1)$$

From Equation 1, if h and A are constant, a smaller ΔT will reduce the heat transfer rate, so the filament will retain more heat to promote polymer bonding. Empirical estimates for h are available for different physical conditions and fluid properties [17]. Equation 1 can be related to specific quantities to determine the amount of heat transferred. This is given by Equation 2 [16]. Q is the amount of heat added (kJ), c_p is the specific heat capacity (kJ/kgK) and m is the mass of heated fluid.

$$Q = \mathrm{m}c_p\Delta\mathrm{T} \quad (2)$$

2.3 Control System

A control system is used to obtain the desired system behaviour. A closed-loop control system uses feedback to automatically regulate a system, whereas an open-loop system requires manual input. An example of a feedback loop in a closed-loop system is shown in Figure 4. A closed-loop control system for ambient temperature control is used in this paper.

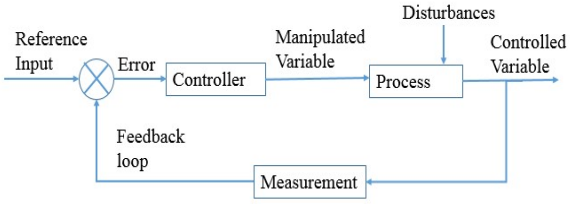

Figure 4: Block diagram of a closed-loop control system

A Proportional Integral Derivative (PID) controller is a type of closed-loop controller widely used in over 95% of industrial processes [18]. For this reason, it was selected to be used for ambient temperature control. A PID controller handles the difference between a measured variable and a desired value by adjusting three separate constant parameters: Proportional (K_P), Integral (K_i), and Derivative (K_d). The PID algorithm that provides the system's response, $u(t)$, is given by Equation 3. $e(t)$ is the error term (the difference between system response and desired value), t is time and x is an integration variable.

$$u(t) = K_P e(t) + K_i \int_0^t e(x)dx + K_d \frac{de(t)}{dt} \quad (3)$$

For the control system used in this paper, the system response varied the power output from a heat source. For a DC driven component, pulse width modulation (PWM) was used to reduce the average power sent to the component, by discretising the signal. Parameter effects on the system response are described in Table II. Values were chosen for the best response to changing temperatures using trial and improvement.

Table 2: PID parameter effects on system response

Parameter	Effect on system response
K_P	Only dependent on the error. Controls how quickly the system responds and its magnitude.
K_i	Sums error over time to balance system response above and below a desired set point. This term will increase the system response until the error is zero and is the most important for PID control.
K_d	Proportional to the rate of change of measured variable to predict the system response.

3. LITERATURE REVIEW

3.1 Heat Environment

Sun et al. (2007) found that print environment temperature and convective currents have the largest effects on bond quality and part mesostructure in FDM [12]. They suggested that better control of these conditions may improve the mechanical properties and accuracy of printed parts. Sun et al. (2007) also noted the limitations of FDM heat transfer models [12]. Models such as those proposed by Li et al. (2002) [10] and Rodriguez et al. (2003) [20], had a limited valid domain due to reliance on experimental data and neglecting conductive heat transfer between adjacent filament trails. Agreeing with Sun et al. (2007), Costa et al. (2014) used FEA software to determine that environment convection and inter-filament conduction had the largest impact on heat transfer [21]. Yan et al. (2000) found that the inter-layer bond strength was dependent on three process parameters: nozzle temperature, heat transfer rate from the part, and the build environment temperature [22]. Gardner et al. (2016) investigated creating a modified desktop printer that could maintain a print environment temperature equal to the glass transition temperature [23]. Reduced part warpage and increased inter-layer adhesion was observed at the cost of increased start-up time.

3.2 Localised Pre-heating

Localised pre-heating uses a heat source to locally increase the print surface temperature prior to filament deposition. This increases inter-layer bonding by providing additional thermal energy. Partain (2007) used a heat gun to investigate improving inter-layer part strength [24]. There was limited reported difference between parts manufactured with additional heat and those manufactured without. Aitchison (2018) similarly investigated via a heat gun the application of hot air to the FDM print surface [25]. It was reported that there was a weak positive correlation between ultimate tensile strength and the top surface temperature of the print, concluding that heat application did increase tensile strength. Kishore et al. (2016) identified weak inter-layer bonding for large scale part production [26]. Infrared lamps were used to preheat the layer prior to deposition and the average fracture energy under low print speeds was found to more than double. Ravi et al. (2016) investigated the effect of using a near infrared laser to locally heat the part surface to above the glass transition temperature prior to filament deposition [27]. The inter-layer bond strength was found to increase by up to 50%. Scanning Electron Microscopy (SEM) analysed the fracture surface of parts and it was concluded that laser pre-heating caused a rougher morphology, providing a higher crack propagation resistance.

3.3 Printer Settings

FDM inter-layer strength can be improved by controlling printer settings. Peng and Wang (2010) investigated flow rate, feed rate and extrusion speed [28]. Part defects were reduced when the ratio of feed rate to flow rate was close to unity. Johansson (2016) investigated printer settings that affected layer bonding performance using a MakerBot Replicator 2X 3D printer [29]. Recommendations for optimal load bearing capacity based on these settings are summarised in Table III. Print settings used in this project were selected using these recommendations and from the author's findings.

Table 3: Print setting recommendations [29]

Print Setting	**Recommendation**
Open vs closed enclosure	Closed
Nozzle temperature	Moderate to high (210°C-250°C)
Flow rate	High (> 1mm/s)
Print layer height	Small (< 0.2 mm)
Print speed	Slow to moderate (<100 mm/s)

3.4 Process Monitoring

Roberson (2016) reviewed FDM sensor-based monitoring literature [30]. Real time process monitoring was found to be inadequately covered. Roberson integrated thermocouples, accelerometers, infrared temperature sensors, and a borescope into a MakerBot Replicator 2X printer for real time process monitoring. Aitchison (2018) used an Arduino microcontroller to monitor hot air applications to investigate its effects on ABS FDM prints [25]. Infrared temperature sensors were used to read print surface temperatures written to a SD card. Bista (2016) carried out work utilising and tuning an Arduino-based PID controller to maintain the temperature of a baby incubator within ± 0.6°C in a laboratory environment [31].

4. METHODOLOGY

4.1 Novelty

The effect of ambient print temperature on inter-layer bond strength in ABS was investigated for a range of temperatures and layer heights. A PID controller operated an external heat source to maintain different enclosure temperatures for a modified MakerBot Replicator 2X 3D printer. The stress-strain relationships, as well as a relationship between ultimate tensile stress (σ_{uts}) and build chamber temperature, were explored using a Lloyd LR5KPlus tensile testing machine. A Dektak 3ST Surface Profilometer measured the vertical profiles of layer heights. A Hitachi S-2400 SEM analysed the surface of parts between layers.

4.2 Heat Source

A DC fan heater was selected to increase printer enclosure temperature. It consisted of a heating element and a small fan to circulate heated air. It was selected for its small size to fit in the enclosure without affecting FDM process movement. Other apparatus such as heat guns and larger fan heaters were not selected due to their high flow rates, which could blow air over the printed part and take heat away. PWM controlled the energy output of the fan heater, as mentioned in Section 2.3. The volume of air in the enclosure was calculated to be 0.0623m^3 and so the mass of air to be heated could be found, given as m in Table 4. The change in temperature that the heater could provide was calculated using Equation 2. Parameters are listed in Table 4, providing a ΔT of 2.3 °C/s if the heater was operated at maximum power. However, this is valid for a thermally insulated enclosure. Section 5.6 explains the ramifications of this in more detail.

Table 4: Heat source calculations

Parameter	Value
Q	0.1 kJ
c_p [32]	1.007 KJ/kg K
m	0.074kg

An open-loop system requires manual input. An example of a feedback loop in a closed-loop system is shown in Figure 4. A closed-loop control system for ambient temperature control was used in this paper.

4.3 Control System

An Arduino UNO microcontroller was chosen to implement PID control due to its low cost and user simplicity. Figure 5 shows a breakdown of the system used to control the ambient air temperature within the print enclosure. It operated at a frequency of 0.2Hz. The system operates by communication from thermocouples to the Arduino microcontroller, facilitating real time temperature capture. Data was written to an SD card with time captured simultaneously. The measured temperature was also passed to a PID control algorithm, which compared it against a desired value. PWM was used to vary the amount of

power sent to the fan heater. The new temperature was then measured by thermocouples, and the process repeated.

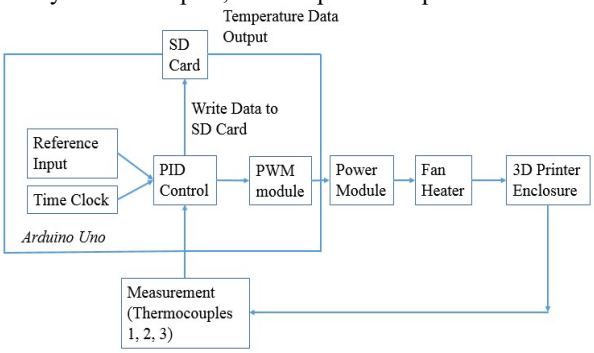

Figure 5: Arduino PID system control

4.4 Experimental Set-up

A MakerBot Replicator 2X 3D printer was used to conduct experiments. It is an enclosed 3D printer and the experimental set-up is shown in Figure 6. Three K-type thermocouples measured ambient print temperature at various locations, which were kept constant for all prints. K-type thermocouples were chosen for their insensitivity to vibration, robustness and location flexibility [33]. They had a resolution of 0.25°C and were calibrated using an accurate thermocouple, discussed more in Section 5.6. The heat source was a fan heater located within the print enclosure so as not to waste energy heating up cold air. It was connected to a DC supply and Arduino circuit. A side panel was designed using CAD and plywood was laser-cut to feed wires. This method provided consistent and repeatable prints.

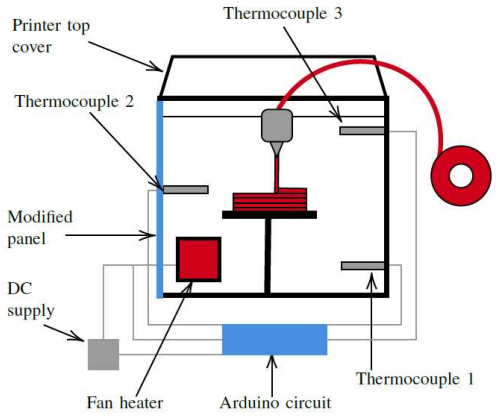

Figure 6: Modified experimental set-up of the makerbot replicator 2X

4.5 Dogbone Tensile Specimen

The dogbone tensile test specimen was designed in CAD using the ISO 527-2:2012 tensile testing standard [34]. This prescribes guidelines such as specimen dimensions for the determination of tensile properties for plastics. Drawings of the test specimen can be found in Figure 7.

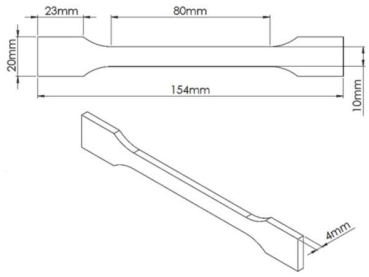

Figure 7: ISO 527-2:2012 dogbone test specimen dimensions [34]

4.6 Print Settings

MakerBot Desktop software was used to slice the CAD dogbone design and prescribe print settings. All print settings were kept constant for prints, with the main settings listed in Table 5. Specimens were printed at two different layer heights with 100% infill to allow cross sectional area (CSA) to be measured when determining stress. Specimens were printed in batches of three to provide multiple samples produced under identical conditions for testing. Parts were printed in an orientation such that the Z-directional strength would be determined through tensile testing. However, this caused the printed parts to have a small footprint on the build plate. This led to instability in the print process, resulting in print failure due to prints falling over from the vibrations and movement of the FDM process. To overcome this, a raft was used. This is printed at the start of the print process before the sliced CAD model. It provides a flat, smooth surface for the print, aiding bed adhesion due to having a larger footprint on the bed.

Table 5: Makerbot desktop main print settings

Print Setting	Value
Extruder temperature	230°C
Print bed temperature	120°C
Layer height	0.2mm & 0.3mm
Infill percentage	100%
Infill Pattern	Linear
Number of shells	7

4.7 Experimental Procedure

The dogbone tensile specimen was printed for the following conditions: open enclosure (printer panels and top cover were removed with no internal heating), closed enclosure (printer panels and top cover in place with no internal heating), and maintaining an internal temperature of 50°C, 55°C, 60°C and 70°C with a closed enclosure. Three test specimens were produced for each condition. This was repeated for each of the two layer heights specified in Table 5. Prints were left to cool slowly to allow an even distribution of internal stresses. Specimen cross-sectional area was measured using Vernier calipers at five constant points across the straight 80mm section shown in Figure 7. This was used to calculate an average cross sectional area for each specimen. The data sampling rate for this machine is 8 kHz with a load cell accuracy of 0.5% [35]. Specimens were tightened at each end in the two gripping jaws

so that there would be no slippage. Care was taken when tightening specimens such that there was no premature fracture or crushing of the specimen. Also, as the specimen was tightened the initial force applied was offset periodically such that the tension applied to the specimen before testing did not exceed 20N. One gripping jaw remained fixed whilst the other was moved away at a constant slow speed of 1mm/min as per ISO 527-2:2012 [34]. Force and extension was measured using the Lloyd LR5KPlus and data extracted as a text file. This procedure was repeated for all three test specimens for each temperature investigated.

5. RESULTS AND DISCUSSION

5.1 Enclosure Temperature Control

As stated in Section 5.7, specimens were produced under different temperature conditions. The open enclosure condition monitored enclosure temperature variations with the print exposed to ambient air conditions. The temperature variation upon printing three 0.3mm layer height dogbone specimens under open enclosure conditions can be found in Figure 8. Temperature was recorded every five seconds; however, data points taken every minute are marked for all temperature plots. This is for clarity and readability. It can be seen that there is a large temperature variation measured by each of the thermocouples primarily due to exposure to changing ambient temperature.

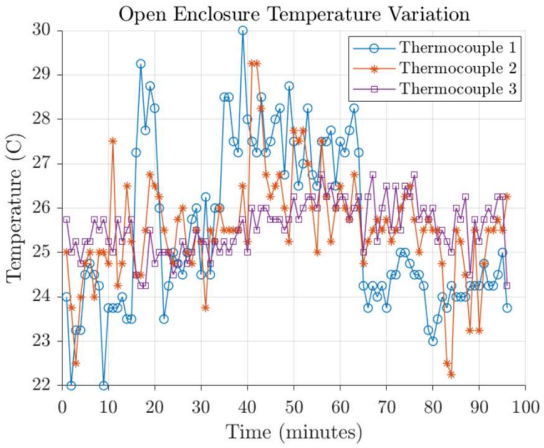

Figure 8: 0.3mm dogbone open enclosure temperature variation

Table 6 gives the maximum, minimum and range of temperatures measured by each thermocouple. There are large variations in print environment temperature, up to 17.5% from the average for thermocouple 1 with a range of 8°C. Similar temperature variations were measured by thermocouple 2 of 7°C. Thermocouple 3 showed the least temperature variation of 2.5°C. This was due to its location in the enclosure, shown in Figure 6. It was located on the inside of the build chamber towards the top, but protected from most of the ambient air temperature change due to the printer frame surrounding it.

Table 6: Open printer enclosure temperature variation

Thermocouple	Max (°C)	Min (°C)	Range (°C)
1	30.00	22.00	8.00
2	29.25	22.25	7.00
3	26.75	24.25	2.50

Furthermore, part quality was significantly reduced because of temperature variations, as shown by Figure 9. In comparison with a closed enclosure print, using the same print settings as specified in Table 5, the open enclosure print has notable distortion. This is particularly prevalent at the top of the print. This could be caused by part warpage in the lower half due to changing ambient air conditions, contributing to a magnified effect observed higher up the print. This demonstrates the need for a build chamber that is isolated from changing ambient air conditions, as noted by Aitchison (2018) [25].

Figure 9: Closed enclosure (left) compared to open enclosure printing (right). Rafts located at the print bases

The closed enclosure printing condition involved side and top panels being reattached to the print enclosure. This provided a more thermally insulated environment that was less affected by changing ambient air conditions. The temperature variations upon printing three 0.3mm layer height dogbone specimens under closed enclosure conditions can be found in Figure 10. The print temperature variations have considerably fewer oscillations than the open enclosure print shown in Figure 8.

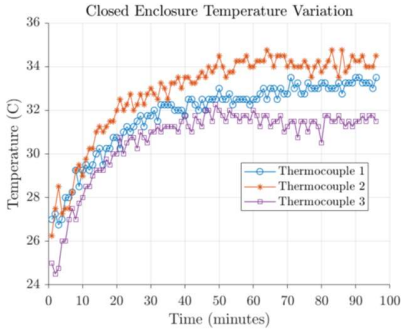

Figure 10: 0.3mm dogbone closed enclosure temperature variation

Table 7 gives the maximum, minimum and range of temperatures measured by each thermocouple. On average, higher temperatures are read by all thermocouples. It can be observed that there are similar large temperature variations during the closed enclosure print compared with Table 6 for the open enclosure, with a trend showing increased temperature measured by all the thermocouples over time. This suggests that part distortion, shown in Figure 9, is influenced by oscillations in the print environment temperature and not by an overall temperature increase. However, the range of temperatures measured by thermocouples for open and closed prints was similar apart from thermocouple 3.

Table 7: Closed printer enclosure temperature variation

Thermocouple	Max (°C)	Min (°C)	Range (°C)
1	33.50	26.75	6.75
2	34.75	26.25	8.50
3	32.25	24.50	7.75

The enclosure temperature increased during the first 40 minutes of the print, as shown in Figure 10. This is caused by the closed enclosure retaining heat produced by the FDM process. As identified in Table 1, the heated print bed is a significant heat source in the FDM process. Moreover, extruder head temperatures are upwards of 230°C during the print process, contributing to the overall heat increase during the FDM process. The temperature stabilises after around 40 minutes due to heat being lost by the enclosure at the same rate it is generated, reaching a thermal equilibrium. For thermocouple 3, a considerably larger range of 7.75°C was recorded for the closed print compared to 2.5°C for the open print. This is due to the aforementioned heat sources within the build chamber. As thermocouple 3 is located towards the top of the print enclosure, it would be expected to record higher temperatures than thermocouples 1 and 2. This is not the case, as can be seen from Table 7. As the print process progresses and the part is built up, the build plate is lowered to accommodate further print layer deposition, as explained in Section 1. The build plate is lowered, increasing proximity to thermocouples 1 and 2, decreasing proximity to thermocouple 3. This causes air to be heated around thermocouples 1 and 2, therefore the recorded temperatures are hotter than thermocouple 3. The moving build plate was a considerable design factor that affected the uniformity of heat distribution during the print process. It is discussed further in Section 5.6.

When tuning PID control parameters, the average enclosure temperature was taken from the three thermocouples. As mentioned previously, there was variation in print environment temperature during the print process, as well as around the enclosure. This meant that it was impossible to heat the print environment such that all areas had the same temperature. Therefore, the goal of temperature control for this project was to achieve an average temperature from the three thermocouples that varied less than 3°C. The temperature variations under 50°C, 60°C and 70°C prints for 0.3mm layer height dogbone specimens are shown in Figure 11. The print environment was heated to reach the desired temperature prior to starting each print. It can be observed that the temperature variation was considerably less than without PID control throughout the whole print. This indicates that PID control was effective, maintaining average desired print temperatures for the whole enclosure. Prints were run at temperatures of 50°C and 55°C for 0.2mm layer height dogbone specimens. It was found that temperature could not be increased higher than 55°C without causing extruder clogging for 0.2mm layer height specimens. This could have been due to the extended time taken to print the specimens and the slower flow rate of filament from the extruder. This caused filament in the extruder head to be at increased temperatures, causing blockages and print failure. This suggests that individual printers may have component dependent limitations for average print temperature.

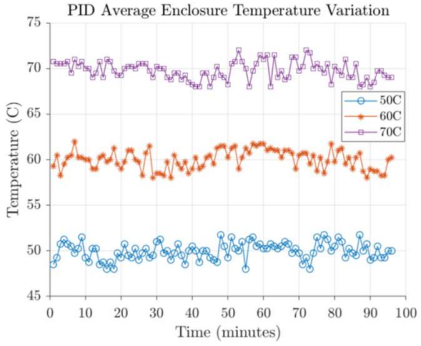

Figure 11: 0.3mm dogbone 50°C, 60°C, 70°C PID average temperature

5.2 Tensile Tests

Force-extension data was read from the Lloyd LR5KPlus tensile testing machine. Cross-sectional areas were calculated by taking dimensional measurements with Vernier calipers for each specimen. Specimens were assumed to be clamped in the same position, providing a constant original specimen length of 113mm. This assumption is discussed further in Section 5.6. Stress and nominal strain were calculated using force-extension data, cross-sectional areas and specimen original length. Stress-strain curves provide a representation of the mechanical material properties of a specimen. Stress-strain curves for 0.3mm and 0.2mm layer height dogbone specimens produced for all print enclosure temperatures can be found in Figure 12 (a) and Figure 12 (b), respectively. Every 25 data points are marked for clarity and readability. The stress-strain curve for the strongest samples for each print temperature are displayed. Specimens failed between layers within the clamped section for all tests and broke cleanly between layers for all but one specimen.

For the majority of all specimen stress-strain curves, Hooke's law of proportionality was obeyed as stress was proportional to strain. As strain was increased, the specimens reached their proportional limit, entering a short plastic flow region. However, as ABS blocks dislocation movement between molecules, which facilitates ductile behaviour, brittle behaviour is observed. After this small section of plastic flow, specimens snapped suddenly at their ultimate tensile stress. Specimens produced with a layer height of 0.2mm, shown in Figure 12 (b),

failed at higher stress levels than those produced with a 0.3mm layer height, shown in Figure 12 (a). This confirms Johansson (2016) [29] findings that a smaller layer height provides stronger inter-layer strength. When conducting tensile testing, dogbone specimens for both layer heights for an open enclosure were deformed at one clamping end. This can be seen from Figure 9. Therefore, it was difficult to ensure that there was no slippage during testing. In Figure 12, both stress-strain curves for open enclosure prints do not follow Hooke's law until yield. This behaviour is not present in specimens produced under different temperature conditions, indicating that open enclosure specimens may have slipped during tensile testing.

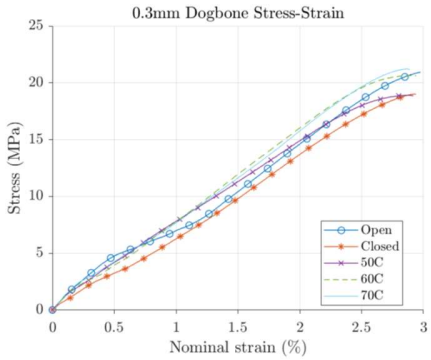

(a) 0.3mm layer height dogbone

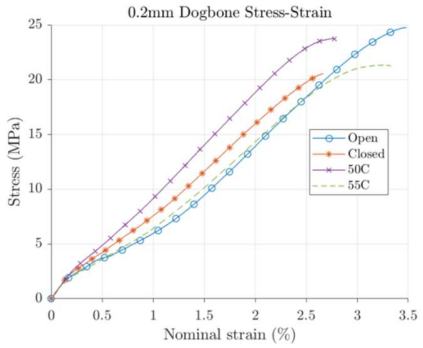

(b) 0.2mm layer height dogbone

Figure 12: dogbone stress-strain curves for all print temperatures

The maximum force each specimen experienced was at breaking, and is represented by F_{max} in Newtons. It was used to calculate the ultimate tensile stress of each specimen through an Engineering definition for stress, given by Equation 4. The ultimate tensile stress of each specimen was plotted against average enclosure temperature, shown in Figure 13.

$$\sigma_{uts} = \frac{F_{max}}{CSA} \quad (4)$$

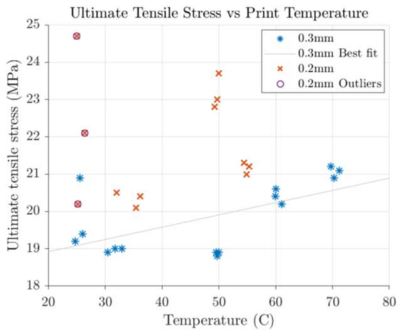

Figure 13: Ultimate tensile stress against average print temperature

Open enclosure specimens were produced at average print temperatures ranging from 24.76°C to 26.43°C. It can be seen that there is a significant range of σ_{uts} for parts produced at these temperatures for both layer heights. As mentioned previously, this is likely to be due to slippage occurring during tensile testing. Outliers exist for 0.2mm layer height dogbones, such as the specimen produced at 24.99°C with σ_{uts} of 24.7 MPa, and are marked on Figure 13. For all other print conditions with specimens produced in a closed enclosure with no external heating, 50°C, 55°C, 60°C and 70°C specimens show clustered behaviour. This indicates that each specimen's σ_{uts} are accurate and reliable. A best fit least squares regression line was calculated for the 0.3mm layer dogbone specimens and is displayed in Figure 13. The highest ultimate tensile stress increase was 10.4% from 19.2 MPa under open enclosure conditions to 21.2MPa under 70°C enclosure ambient temperature. This indicates a weak positive relationship between average print temperature and ultimate tensile stress, supporting the hypothesis that increasing ambient air temperature increases part strength in the Z-direction. Such a relationship cannot be stated for the 0.2mm layer height dogbone specimens due to open enclosure outliers and insufficient temperature range for data collected.

5.3 Dektak Surface Profilometer

A Dektak 3ST surface profilometer measured the vertical profiles of specimens by moving a stylus over the specimen surface and recording displacement. It provides an insight into how specimen layers are separated. A comparison between an open enclosure dogbone specimen and a 50°C enclosure one, for 0.2mm layer height, can be found in Figure 14. Every five data points are marked on the plot for clarity and readability. The X-axis of the plot measures distance along the length of the sample in micrometers (10^{-6}m) and the Y-axis measures the vertical profile of the sample in Kilo Angstroms (10^{-7}m). Each peak represents the top of a layer, whereas each trough represents the boundary between layers. The open print has a higher plot amplitude than the 50°C print and there is less distinction between layers for the specimen produced at 50°C. It indicates that boundaries between layers for the open print are more distinct, and could suggest why the ultimate tensile stress was lower for the 0.2mm open prints compared to those produced at 50°C. This suggests that prints produced at higher temperatures

have less boundary distinction between layers, due to greater polymer inter-diffusion between trails, hence why an increase in Z-directional strength is shown in Figure 13.

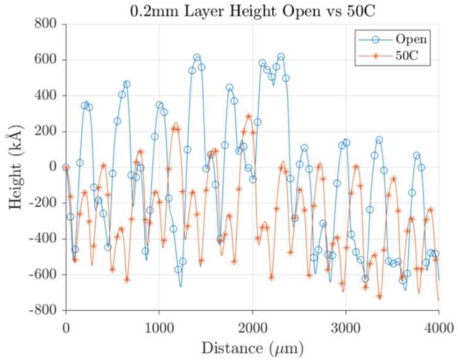

Figure 14: 0.2mm Dektak open vs 50°C height comparison

5.4 SEM

A Hitachi S-2400 SEM was used to analyse specimen surface between layers. Images of part morphology are formed by scanning a focused electron source over the specimen. The surface morphology of a 0.3mm dogbone specimen produced under open and 70°C enclosure conditions can be seen in Figures 15 (a) and (b), respectively. It can be observed that at 500 μm, the surface layer appears smoother and less defined in Figure 15 (b), indicating that more polymer inter-diffusion has occured. Figure 13 shows that the strength of parts produced at 70°C is higher than those produced with an open enclosure for the 0.3mm dogbone specimen. This reinforces the hypothesis that increasing ambient print temperature causes more polymer inter-diffusion and therefore a stronger Z-directional strength.

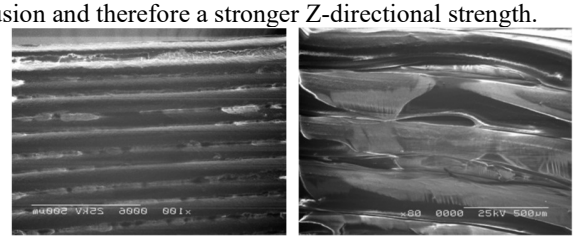

(a) (b)

Figure 15: SEM 0.3mm dogbone produced under (a) open and (b) 70°C enclosure conditions at 500μm scale

5.5 Thermal Camera

A thermal camera was used to inspect heat application uniformity and heat distribution, and identify heat loss in the FDM process. A thermal image taken during the printing process is shown in Figure 16. As mentioned in Section 5.1, it was impossible to ensure every part of the enclosure was the same temperature due to the moving build plate. The lower half of the enclosure is approximately 10°C cooler than the top half. Around the enclosure side panels the temperature is lower, indicating that heat has been lost. This is particularly apparent at the top and front of the enclosure, where Perspex panels sealed the enclosure. For future experimentation a more thermally insulated enclosure is advised.

Figure 16: Thermal image of heat distribution at the start of a print

5.6 Errors

Calibration of thermocouples was necessary as their response depends on the composition of materials used to construct them. A water boiling calibration test was conducted using an accurate thermocouple and a K-type thermocouple was used during experimentation. Water was slowly heated to boiling with temperature logged each second, shown in Figure 17, with markers placed every 50 data points. Regression analysis was performed to minimise residuals and an equation was found to translate the K-type thermocouple data.

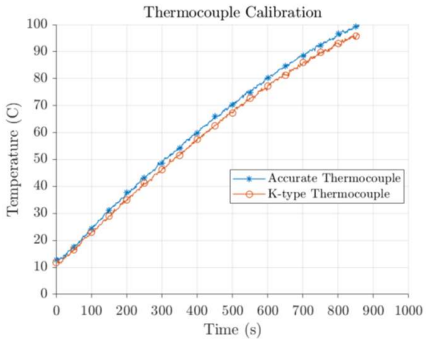

Figure 17: K-type thermocouple boiling ice water calibration

As noted in Section 4.2, calculations performed to ensure the DC fan heater could raise the enclosure temperature did not take into account the amount of heat lost through the Perspex printer top cover and side panels. As a result, a heat gun was required to help raise enclosure temperature for the 70°C print. This required manual input. A more powerful enclosure heater is advised in future experiments, potentially in conjunction with adding additional thermal insulation to the printer.

Metal Vernier calipers were zeroed and used to measure specimen cross-sectional area at a precision of 0.01mm. Taking an example of a cross-sectional area measured as 42.33mm^2, the error associated with this is 0.175%, which was deemed acceptable. When calculating nominal strain, it was assumed that specimens were clamped in the same location each time with a constant original length of 113mm. This may have had a large impact on the stress-strain curves produced.

Finally, as mentioned in Section 4.1, it was impossible to ensure the entire printer enclosure was the same temperature due to the Z-directional moving build plate. The solution to this is to

use more temperature sensors around the enclosure, providing a more accurate value of the enclosure temperature.

6. CONCLUSIONS

This paper investigated increasing Z-directional anisotropic part strength in FDM. It was found that the key to increasing inter-layer part strength is through increasing inter-layer polymer bonding, which is driven by thermal fusion and polymer inter-diffusion of extruded material [12]. It was hypothesised that if heat transfer away from the printed part was reduced, more heat would be available to drive this bonding process, leading to stronger inter-layer part strength. In literature, there was no reference to ambient temperature control to reduce heat convection over a range of temperatures for ABS prints in FDM. An Arduino-based PID controller was used to maintain ambient print temperature using a DC fan heater. Guidelines for the tensile testing of plastics from ISO 527-2:2012 were followed. Three K-type thermocouples were used to measure ambient print temperatures at various locations, kept constant for all prints. There were large open and closed enclosure temperature variations of up to 8°C with oscillatory behaviour and part distortion present. Enclosure print temperatures of 50°C, 55°C, 60°C and 70°C were investigated. It was found that for 0.3mm layer height dogbone specimens printed at 70C, part strength increased by a maximum of 10.4% compared to open enclosure printing. A weak positive correlation between Z-directional part strength and ambient print temperature could be concluded for 0.3mm dogbones, but not for 0.2mm dogbones due to insufficient data. This was due to specimen slippage during tensile testing. A Dektak surface profilometer indicated that layer boundaries are less distinct when prints are produced in a higher temperature environment, due to increased polymer inter-diffusion between trails. SEM showed that at 500 µm surface morphology is smoother with less defined boundaries between layers for specimens printed at higher ambient air temperatures, suggesting more polymer inter-diffusion has occurred, reinforcing the hypothesis of this paper.

Increasing ambient print temperature has yielded promising results in terms of increasing Z-directional part strength. Useful further work would involve additional experimentation at a wider range of temperatures to find an ideal printing temperature that may be dependent on print settings and the printer used. For further experimentation, a more powerful enclosure heater, extra thermocouples to measure temperature variation in the print enclosure, and an improved thermally insulated print enclosure would be required.

REFERENCES

[1] E. Matias and B. Rao, “3D printing: On its historical evolution and the implications for business,” 2015 Portland International Conference on Management of Engineering and Technology, pp. 551–558, 2015.

[2] M. Attaran, “The rise of 3-D printing: The advantages of additive manufacturing over traditional manufacturing,” Business Horizons, vol. 60 (5), pp. 677–688, 2017.

[3] N. Ahmed and J. Page, “Manufacture of an unmanned aerial vehicle (UAV) for advanced project design using 3D printing technology,” Applied Mechanics and Materials, vol. 397, pp. 970–980, 2013.

[4] A. Capel, R. Rimington, M. Lewis, and S. Christie, “3D printing for chemical, pharmaceutical and biological applications,” Nature Reviews Chemistry, vol. 4, pp. 422–436, 2018.

[5] Q. Yan, H. Dong, J. Su, J. Han, B. Song, Q. Wei, and Y. Shi, “A review of 3D printing technology for medical applications,” Engineering, vol. 5, pp. 729–742, 2018.

[6] “3D printed parts and new materials help Rolls-Royce to engine test success,” https://www.rolls-royce.com/media/press-releases/2018/11-10-2018-3-d-printed-parts-and-new-materials-help-rolls-royce-to-engine-test-success.aspx, accessed: 2020-05-11.

[7] “The 9 Different Types of 3D Printers,” https://3dinsider.com/3d-printertypes/, accessed: 2020-05-11.

[8] “Introduction to FDM 3D printing,” https://www.sdhubs.com/knowledge-base/introduction-fdm-3d-printing, accessed: 2020-05-11.

[9]“What is FDM Technology?” https://www.stratasys.com/fdm-technology, accessed: 2020-05-11.

[10] L. Li, Q. Sun, C. Bellehumeur, and P. Gu, “Composite modeling and analysis for fabrication of FDM prototypes with locally controlled properties,” Journal of Manufacturing Process, vol. 14, pp. 129–132, 2002.

[11] “3D printed components to be tested on passenger trains,” https://www.railwaygazette.com/news/technology/single-view/view/3dprinted-components-to-be-tested-on-passenger-trains.html, accessed: 2020-05-11.

[12] Q. Sun, G. Rizvi, C. Bellehumeur, and P. Gu, “Effect of processing conditions on the bonding quality of FDM polymer filaments,” Rapid Prototyping Journal, vol. 14, pp. 72–80, 2008.

[13] S. Ahn, M. Montero, D. Odell, S. Roundy, and S. Wright, “Anisotropic material properties of fused deposition modeling ABS,” Rapid Prototyping Journal, vol. 8, pp. 248–257, 2002.

[14] J. Choi, J. Ryu, and K. S., “Korea-Australia Rheology Journal,” Department of Fiber and Polymer Science, Seoul National University, vol. 12, pp. 135–141, 2000.

[15] T. McLeish, “Tube theory of entangled polymer dynamics,” Advances in Physics, vol. 51, pp. 1379–1527, 2002.

[16] S. Kakac and Y. Yener, “Convective Heat Transfer, Second Edition,” CRC Press, 1995.

[17] “Isis Steam Typical Overall Heat Transfer Coefficients,” http://www.isissteam.com/downloads/heat-transfer.pdf, accessed: 2020-05-11.

[18] J. Astrom and H. Hagglund, “New tuning methods for PID controllers,” Proceedings of the 3rd European Control Conference, 1995.

[19] “Introduction: PID Controller Design,” http://ctms.engin.umich.edu/CTMS/index.php?example=Introduction&section=ControlPID, accessed: 2020-05-11.

[20] J. Rodriguez, J. Thomas, and J. Renaud, “Mechanical behavior of acrylonitrile butadiene styrene fused deposition

materials modeling," Rapid Prototyping Journal, vol. 9, pp. 219–230, 2003.
[21] S. Costa, F. Duarte, and J. Covas, "Thermal conditions affecting heat transfer in FDM/FFE: a contribution towards the numerical modelling of the process," Institute for Polymers and Composites, Department of Polymer Engineering University of Minho, GuimarÃˇces, Portugal, 2014.
[22] Y. Yan, R. Zhang, G. Hong, and X. Yuan, "Research on the bonding of material paths in melted extrusion modeling," Materials & Design, vol. 21, pp. 93–99, 2000.
[23] J. Gardner, C. Stelter, E. Yashin, and E. Siochi, "High temperature thermoplastic additive manufacturing using low-cost, open-source hardware," NASA STI Program, 2016.
[24] S. Partain, "Fused deposition modeling with localized pre-deposition heating using forced air," Montana State University Master's Thesis, 2007.
[25] A. Aitchison, "Localised pre-heating to improve inter-layer delamination strength in fused deposition modelling," Durham University Master's Thesis, 2018.
[26] V. Kishore, C. Ajinjeru, A. Nycz, B. Post, J. Lindahl, V. Kunc, and C. Duty, "Infrared preheating to improve interlayer strength of big area additive manufacturing (BAAM) components," Additive Manufacturing, vol. 14, pp. 7–12, 2017.
[27] A. Ravi, A. Deshpande, and K. Hsu, "An in-process laser localized pre-deposition heating approach to inter-layer bond strengthening in extrusion based polymer additive manufacturing," Journal of Manufacturing Processes, vol. 24, pp. 179–185, 2016.
[28] A. Peng and Z. Wang, "Researches into influence of process parameters on fdm parts precision," Applied Mechanics and Materials, vol. 34, pp. 338–343, 2010.
[29] F. Johansson, "Optimizing fused filament fabrication 3D printing for durability," Blekinge Institute of Technology Master's Thesis, 2016.
[30] D. Roberson III, "Sensor-based online process monitoring in advanced manufacturing," Virginia Polytechnic Institute and State University Master's Thesis, 2016.
[31] D. Bista, "Understanding and design of an arduino-based pid controller," Masters of Science at Virginia Commonwealth University, 2016.
[32] "Penn State College of Engineering, Properties of air at 1 atm pressure," https://www.mne.psu.edu/cimbala/me433/Links/Table_A_9_CC_Properties_of_Air.pdf, accessed: 2020-05-11.
[33] "Omega Engineering: Temperature probes," https://www.omega.co.uk/temperature/z/thermocouple-RTD.html, accessed: 2020-05-11.
[34] "International Organization for Standardization:ISO 527-2:2012," https://www.iso.org/standard/56046.html, accessed: 2020-05-11.
[35] "Lloyd LR5KPlus Materials Testing Machine Datasheet," https://www.ametektest.com/-media/ametektest/download_links/data_dual_column_test_stands_lr5kplus_data_sheet_english.pdf, accessed: 2020-05-11.